Journal of Catalysis **204,** 98–109 (2001)
doi:10.1006/jcat.2001.3387, available online at http://www.idealibrary.com on IDEAL®

Co-Support Compound Formation in Alumina-Supported Cobalt Catalysts

Bunjerd Jongsomjit,* Joongjai Panpranot,† and James G. Goodwin, Jr.†,[1]

*Department of Chemical and Petroleum Engineering, University of Pittsburgh, Pittsburgh, Pennsylvania 15261; and †Department of Chemical Engineering, Clemson University, Clemson, South Carolina 29634

Received March 8, 2001; revised August 10, 2001; accepted August 10, 2001

In supported cobalt catalysts, the formation of cobalt-support compounds can result in lower activity of the catalysts. It has been found that water vapor present during standard reduction affects the degree of reducibility of cobalt in CoRu/γ-Al_2O_3. In this study, the impact of water vapor on the formation of Co-support compounds and the resulting characteristics of Co/γ-Al_2O_3 and Co-Ru/γ-Al_2O_3 catalysts were investigated to develop a better understanding of the nature of the Co-support compounds formed and the effect of noble metal promotion on their formation. The Co catalysts were reduced under differential conditions with and without added water vapor and then characterized. Co-support compound formation could not be detected by X-ray diffraction; however, Raman spectroscopy gave useful information about the Co "aluminate" formed. Temperature-programmed reduction indicated that the degree of reduction of the catalyst samples was lower when additional water vapor was introduced during reduction, but to a lesser degree when the Ru promoter was present. The Raman spectroscopic results suggest that the Co aluminate formed is not identical to $CoAl_2O_4$ (spinel) but is probably a surface compound deficient in Co. This compound formation is a major cause for differences seen in the degree of reducibility of Co/alumina catalysts after initial reduction, hydrogen chemisorption capacity, and Fischer–Tropsch synthesis activity.

1. INTRODUCTION

The Fischer–Tropsch (F–T) synthesis provides a means of converting coal and natural gas to petrochemicals and liquid transportation fuels. Supported cobalt (Co) catalysts are the preferred catalysts for F–T synthesis based on natural gas because of their high F–T activity (1), high selectivity for linear hydrocarbons, low activity for the water gas shift reaction (2, 3), and lower cost compared to Ru (4). However, compound formation between cobalt metal and the support can occur under pretreatment and/or reaction conditions (5–7), leading to irreversible catalyst deactivation.

The effects of noble metal promoters such as Ru (8–10), Rh (11, 12), and Pt (13) on cobalt-based catalysts have been investigated. It has been proposed that these metal promoters can increase the reducibility and dispersion of Co (8, 13–15), preserve the activity by preventing the formation of coke (16), exhibit cluster and ligand effects (17), and act as a source for hydrogen spillover (4).

In a previous temperature-programmed reduction (TPR) study reported from our laboratory, Zhang *et al.* (7) investigated the reducibility of CoRu/γ-Al_2O_3 during standard reduction and during TPR in the presence of added water vapor. It was confirmed that water has a significant effect on the reduction behavior of CoRu/γ-Al_2O_3. It was suggested that water vapor present during standard reduction leads to a decrease in the degree of reduction of the cobalt in two possible ways: (i) inhibition of the reduction of well-dispersed CoO interacting with the alumina support, possibly by increasing the cobalt–alumina interaction, and (ii) facilitation of the migration of cobalt ions into probable tetrahedral sites of γ-Al_2O_3 to form a nonreducible (at temperatures $<900^\circ$C) spinel. This irreversible compound formation results in a decrease in the amount of reducible cobalt metal atoms using conventional reduction procedures. Although the effect of water vapor on reducibility during standard reduction and TPR was studied, the nature of the Co-support compounds formed were not identified due to the limitations of the experimental techniques used.

It is known that water vapor is a by-product of metal catalyst reduction. In a laboratory, the amount of water can be minimized; but during reduction of the catalyst on an industrial scale, this is more difficult. Thus, we need to understand the impact of water on cobalt-support compound formation and how it can be minimized during catalyst reduction and subsequent reaction.

The nature of Co-support compound formation and its effect on the characteristics of the catalysts were the focus of the present research. It is very important to fully understand the impact of water vapor on the formation of Co-support compounds and their nature in order to develop a strategy to minimize their formation. The main objectives of this study were to develop further knowledge about Co-support compound formation during reduction, to better identify the compounds formed, and to investigate

[1] To whom correspondence should be addressed. Fax: (864)-656-0784. E-mail: james.goodwin@ces.clemson.edu.

0021-9517/01 $35.00

the effect of noble metal (Ru) promotion on Co-support compound formation. In the present study, Co/γ-Al_2O_3 and CoRu/γ-Al_2O_3 catalysts were pretreated under various conditions and were then characterized using Brunauer–Emmett–Teller (BET), X-ray diffraction (XRD), scanning electron microscopy (SEM), energy-dispersive X-ray spectroscopy (EDX), Raman spectroscopy, TPR, and H_2 chemisorption.

2. EXPERIMENTAL

2.1. Catalyst Preparation

2.1.1. Co/γ-Al_2O_3. The Co/γ-Al_2O_3 catalyst was prepared using the incipient wetness impregnation of γ-Al_2O_3. The support precursor (Al_2O_3, Vista B) was first calcined at 500°C for 10 h before impregnation in order to put it in the form of γ-Al_2O_3 having a specific surface area of 209 m^2/g and an average particle size ca. 60 μm. Cobalt nitrate ($Co(NO_3)_2 \cdot 6H_2O$) was dissolved in deionized water and impregnated into the support using incipient wetness to give a final reduced catalyst with 20 wt% cobalt. The catalyst was dried at 110°C for 12 h and calcined in air at 300°C for 2 h.

2.1.2. CoRu/γ-Al_2O_3. The CoRu/γ-Al_2O_3 catalyst was also prepared by the incipient wetness coimpregnation method. The same γ-Al_2O_3 support as mentioned before was used. Cobalt nitrate and ruthenium(III) nitrosyl nitrate ($Ru(NO)(NO_3)_3$) were dissolved in deionized water and coimpregnated into the support to produce a reduced catalyst with 20 wt% cobalt and 0.5 wt% ruthenium. The catalyst was also dried at 110°C for 12 h and calcined in air at 300°C for 2 h.

2.1.3. $CoAl_2O_4$ (spinel), CoO, and Co_3O_4 (spinel). In order to identify the Raman bands and XRD peaks of the samples, cobalt aluminate (spinel) [98% $CoAl_2O_4$, 39–41% Co], cobalt(II) oxide [95% CoO] from Alfa Aesar, and cobalt(II, III) oxide [99.5% Co_3O_4] from Strem Chemicals, Inc., were used as reference materials.

2.2. Catalyst Pretreatment

The catalysts were characterized following three pretreatments. These were as follows:

(i) after the original calcination step;

(ii) after standard reduction of the calcined catalysts in a high space velocity (16,000 h^{-1}) of H_2 at 350°C for 10 h and passivation with an O_2/He (5.20% of O_2) mixture at room temperature for 2 h;

(iii) after standard reduction of the calcined catalysts in a high space velocity (16,000 h^{-1}) of H_2 with 3% added water vapor at 350°C for 10 h followed by passivation with an O_2/He (5.20% of O_2) mixture at room temperature for 2 h.

While the concentration of water vapor during reduction without added water vapor was certainly not zero, it was very low due to the high space velocity used.

2.3. Catalyst Nomenclature

The following nomenclature was used for samples in this study. *C* is the calcined catalyst samples, *RP* is the reduced and passivated catalyst samples, and *RWP* is the catalyst samples reduced in H_2 with 3% added H_2O vapor and then passivated.

2.4. Catalyst Characterization

2.4.1. BET surface area. BET surface area measurements were performed to determine if the total surface area changes following different pretreatment conditions. The surface area was determined using N_2 adsorption at 77 K in a Micromeritics ASAP 2010.

2.4.2. X-ray powder diffraction. XRD was performed to determine the bulk crystalline phases of the catalysts following different pretreatment conditions. X-ray powder diffraction patterns of samples were collected using a Philips X'pert X-ray diffractometer with monochromatized CuK_α radiation ($\lambda = 1.54439$ Å). The spectra were scanned at a rate of 2.4 degree/min in the range $2\theta = 20$–80 degrees.

2.4.3. Raman spectroscopy. The Raman spectra of the samples were collected by projecting a continuous wave laser of argon ion (Ar^+) green (514.532 nm) through the samples exposed to air at room temperature. A scanning range between 0 and 1000 cm^{-1} with a resolution of 2 cm^{-1} was applied. The data were analyzed using the Renishaw WiRE (Windows-based Raman Environment) software, which allows Raman spectra to be captured, calibrated, and analyzed using system 2000 functionality via the Galactic GRAMS interface with global imaging capacity.

2.4.4. Scanning electron microscopy and energy-dispersive X-ray spectroscopy. Particle microstructure and elemental distribution were determined using SEM and EDX, respectively. SEM and EDX analysis were performed using a Philips XL30 FEG electron microscope. SEM micrographs were further analyzed using Scion Beta 2 image analysis software for determination of areas and perimeters of particle projections. Elemental distribution data were further analyzed using EDAX software.

2.4.5. Hydrogen chemisorption. Static H_2 chemisorption at 100°C on the reduced cobalt catalysts (re-reduced at 350°C) was used to determine the number of reduced surface cobalt metal atoms. This is related to the overall activity of the catalysts during Fischer–Tropsch Synthesis (FTS). Gas volumetric chemisorption at 100°C was performed using the method described by Reuel and Bartholomew [18]. The experiment was performed in a Micromeritics ASAP 2010 using ASAP 2010C V3.00 software.

2.4.6. Temperature programmed reduction. TPR was performed to determine the reducibilities of the catalyst samples. TPR was carried out in an Altamira AMI-1 system. It was conducted using 50 mg of catalyst and a temperature ramp from 30 to 900°C at 5°C/min. The carrier gas was 5% H_2 in Ar. A cold trap (−70°C) was placed before the detector to remove water produced during the reaction. A thermal conductivity detector was used to determine the amount of hydrogen consumed. The hydrogen consumption was calibrated using TPR of silver oxide (Ag_2O) at the same conditions. The *RP* and *RWP* catalyst samples were recalcined at the original calcination conditions before performing TPR.

2.5. Reaction

FTS was carried out at 220°C and 1 atm total pressure. A flow rate of $H_2/CO/Ar = 60/30/10$ cm^3/min in a fixed-bed reactor under differential conditions was used. Thermocouples at the top and the bottom of the catalyst bed assured precise temperature control during pretreatment and reaction. Typically, 0.2 g of the pretreated catalyst sample was re-reduced *in situ* in flowing H_2 (50 cc/min) at 350°C for 10 h prior to FTS. In order to avoid exotherms and hot spots that lead to rapid catalyst deactivation, the reaction was initiated in a controlled manner by gradually increasing the reactant concentrations over a period of 2 h. After the start-up, samples were taken at 3-h intervals and analyzed by gas chromatography. Steady state was reached after 24 h in all cases.

3. RESULTS

3.1. BET Surface Area

BET surface areas of the Co catalysts after various pretreatments were all slightly less than that of the alumina support (209 m^2/g). Since all the surface areas of the catalyst samples in this study ranged between 171 and 188 m^2/g, there was no significant change in surface areas after the various pretreatments within experimental error.

3.2. X-ray Diffraction

XRD patterns of the Co and CoRu catalysts following different pretreatment conditions are shown in Fig. 1. The calcined samples of Co-*C* and CoRu-*C* had identical XRD patterns. The diffraction peaks at 31.3°, 36.8°, 59.4°, and 65.4° are those of Co_3O_4. The XRD patterns of reduced and passivated samples of Co-*RP*, Co-*RWP*, CoRu-*RP*, and CoRu-*RWP* were also essentially identical. The diffraction peaks at 42.6° and 61.8° in both catalyst series were due to CoO. No peaks for Co metal were seen in any of the XRD patterns due to overlap with those for γ-Al_2O_3. For reference, XRD of the alumina support, CoO, $CoAl_2O_4$ (spinel), and Co_3O_4 (spinel) was carried out, and their XRD patterns

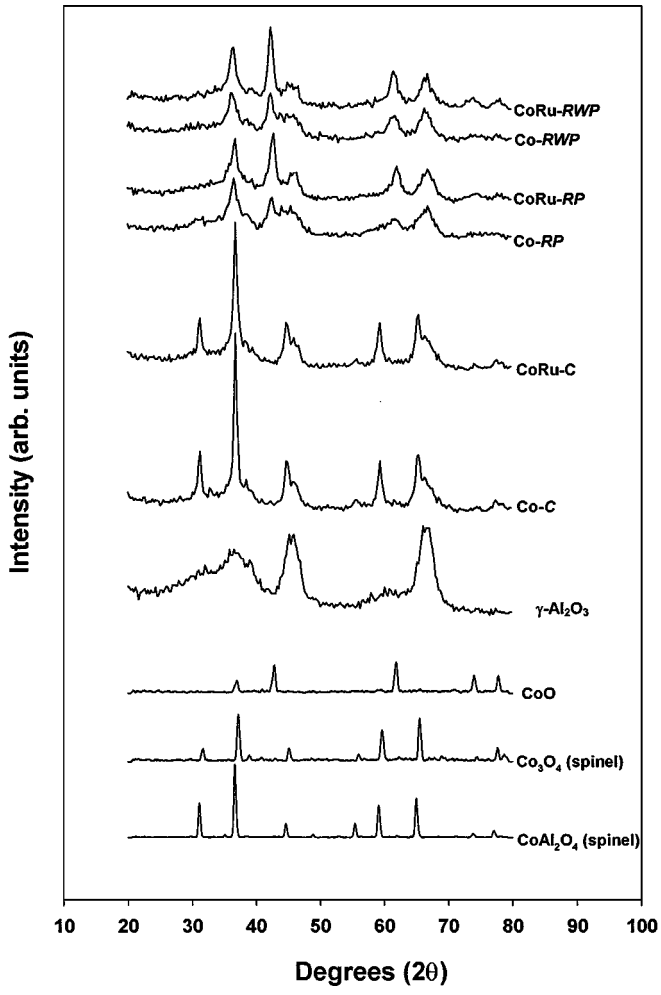

FIG. 1. XRD patterns of γ-Al_2O_3, CoO, Co_3O_4 (spinel), $CoAl_2O_4$ (spinel), Co/γ-Al_2O_3, and CoRu/γ-Al_2O_3 after different pretreatments.

are also shown in Fig. 1. No peaks for $CoAl_2O_4$ (spinel) were detected for any of the catalyst samples.

3.3. Raman Spectroscopy

Raman spectra for Co and CoRu catalysts after different pretreatment conditions are shown in Fig. 2. Strong Raman bands for Co-*C* and CoRu-*C* were observed at 694, 528, and 488 cm^{-1}, which can be assigned to Co_3O_4 (19, 20). Raman bands for Co_3O_4 were not apparent for Co-*RP*, Co-*RWP*, CoRu-*RP*, or CoRu-*RWP* because of its reduction to CoO and Co metal. Broad Raman bands between 400 and 750 cm^{-1} could be observed in the reduced and passivated samples of Co-*RP*, Co-*RWP*, CoRu-*RP*, and CoRu-*RWP*. However, the peak area in that region was significantly more apparent when 3% added water vapor was present during standard reduction. For the same pretreatment conditions, the broad peak in that region was apparently diminished when Ru promotion was used. In order to identify the Raman bands of the samples, Raman spectra of bulk CoO,

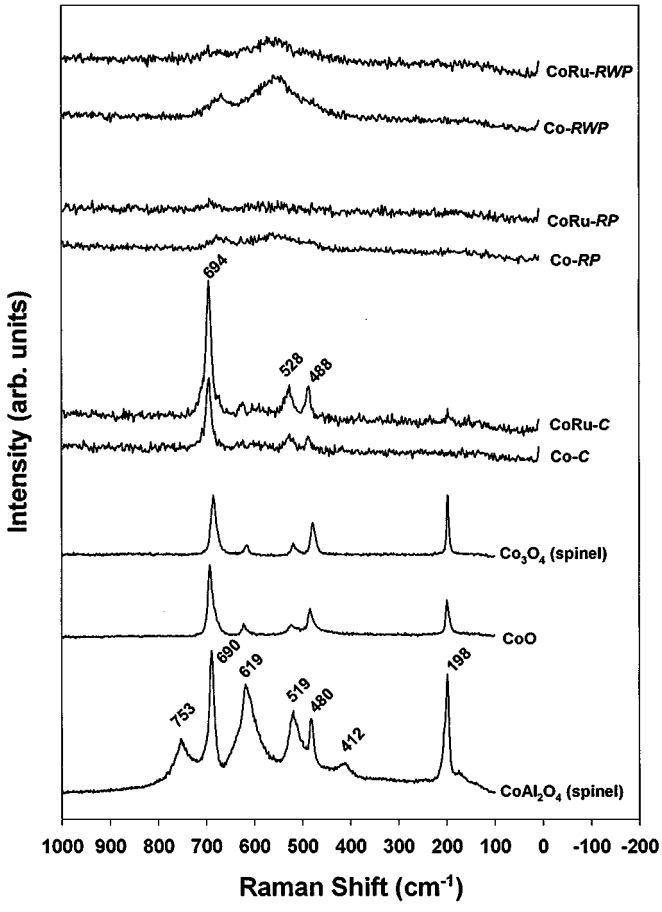

FIG. 2. Raman spectra of Co/γ-Al_2O_3 and CoRu/γ-Al_2O_3 after different pretreatments, CoO, Co_3O_4 (spinel), and $CoAl_2O_4$ (spinel).

Co_3O_4 (spinel), and $CoAl_2O_4$ (spinel) were collected; these are also shown in Fig. 2. It indicates that $CoAl_2O_4$ (spinel) has strong Raman bands at 198, 412, 480, 519, 619, 690, and 753 cm^{-1}. The broad Raman bands of the catalyst samples between 400 and 750 cm^{-1} are clearly not identical to those of $CoAl_2O_4$ (spinel), CoO, or Co_3O_4.

3.4. Scanning Electron Microscopy

SEM micrographs of Co and CoRu after different pretreatment conditions are shown in Figs. 3 to 6. The term granule is used here to refer to the overall catalyst particles composed of Co, Ru (for CoRu), and γ-Al_2O_3. The term patches is used to refer to entities rich in Co supported on the catalyst granules. In all the SEM figures, the white or light spots on the catalyst granules represent high concentrations of cobalt and its compounds, while the darker areas of the granules indicate the support with minimal/no cobalt present. Figures 3 and 4 show SEM micrographs of the catalysts after initial calcination (Co-*C* and CoRu-*C*) on the carbon tapes used for holding the catalyst samples (the dark background). Figure 3 shows the typical overall shapes of the granules of the catalysts studied. It can be seen in Fig. 4 that Co on the CoRu catalyst granules was more dispersed (i.e., smaller SEM-visible patches/particles) than on the unpromoted Co catalyst. The morphologies of the catalyst granules changed insignificantly for the most part after the different reduction conditions (not shown here). However, the most dramatic change is shown in Fig. 5. As can be seen, there was a significantly greater number of small Co patches/particles on Co-*RP* granules than on Co-*RWP* ones. This same phenomenon was also observed for CoRu-*RP* and CoRu-*RWP*, as shown in Fig. 6.

3.5. Temperature Programmed Reduction

TPR profiles of bulk Co_3O_4 and the Co and CoRu catalysts after different pretreatment conditions are shown in Fig. 7. As can be seen in the figure, one reduction peak envelop for bulk Co_3O_4 was obtained. This can be assigned to the two-step reduction of Co_3O_4 to CoO and then to Co^0 (7, 13, 21).

There were three major reduction peaks for Co-*C* located at ca. 200°, 300°, and between 400° and 750°C (maximum at 600°C). These peaks have been related to the following steps: decomposition of residual Co nitrate, $Co_3O_4 \rightarrow CoO$, $CoO \rightarrow$ Co metal, and Co_XO_Y–$Al_2O_3 \rightarrow$ Co metal (8, 13, 22, 23). However, after reduction, passivation, recalcination, and TPR, there were only two peaks left for Co-*RP* and Co-*RWP*, located at ca. 350°C and between 400 and 750°C.

For the CoRu catalyst after different pretreatment conditions, there were always only two peaks. For CoRu-*C*, these were located at ca. 200°C and between 250° and 550°C (max. at 400°C). After reduction, passivation, recalcination, and TPR, two peaks of reduction were still observed for CoRu-*RP* and CoRu-*RWP*. However, they were located at slightly higher temperatures: ca. 250°C and between 300° and 600°C.

The reducibilities of the catalyst samples after different pretreatments are shown in Table 1. They ranged from 83 to 50% for the Co catalyst and from 98 to 80% for CoRu. The reducibilities of catalyst samples decreased with the introduction of 3% additional water vapor during reduction and increased with the addition of the Ru promoter.

3.6. Hydrogen Chemisorption

The H_2 chemisorption results for Co and CoRu after different pretreatment conditions are shown in Table 1. The overall dispersion of reduced Co in the catalyst samples and the average reduced Co metal particle sizes are also given. The results indicate that the overall dispersion increases with the addition of Ru promoter (5.7–7.8%) and decreases with the introduction of water vapor during reduction, especially in the absence of the Ru promoter (5.7–3.8%).

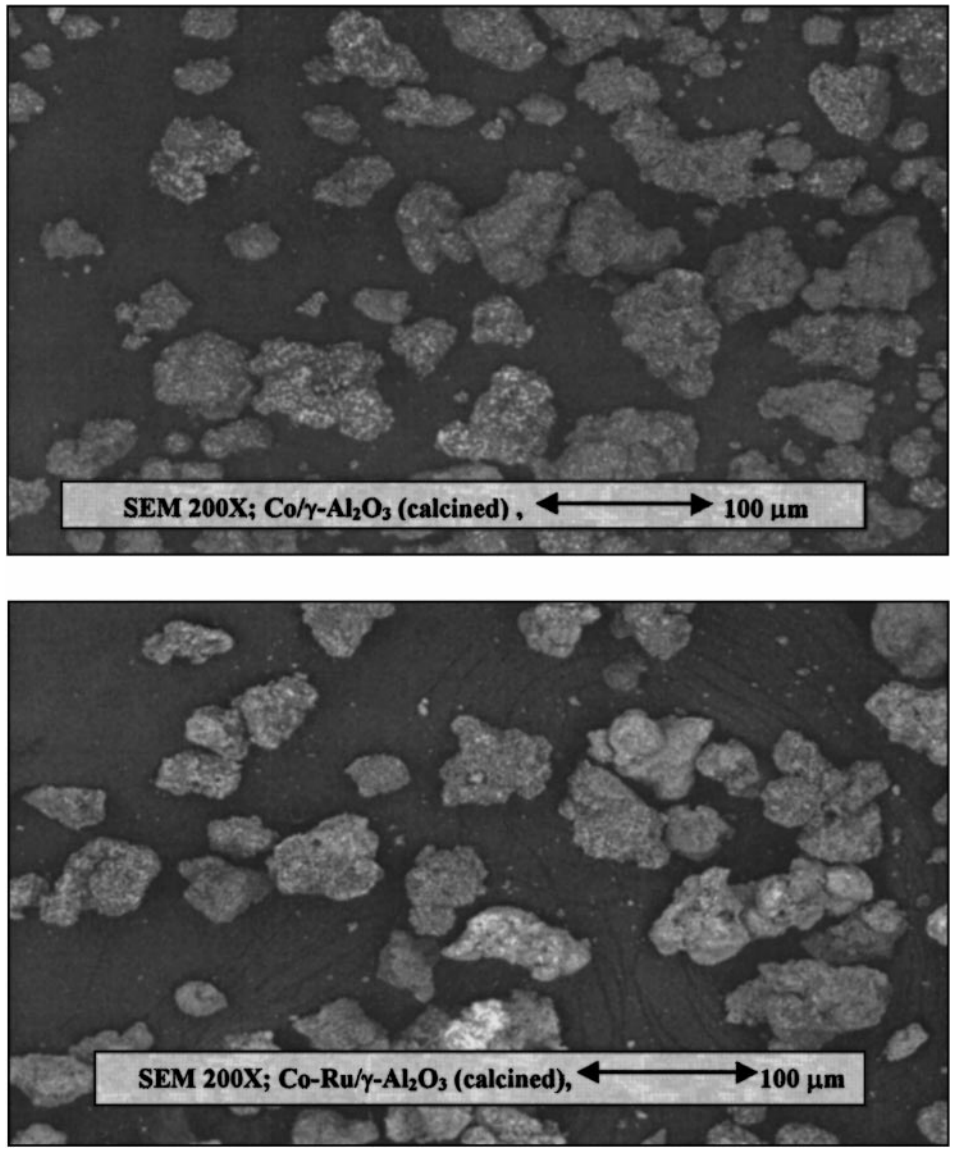

FIG. 3. SEM of the calcined Co/γ-Al_2O_3 and CoRu/γ-Al_2O_3 catalysts at 200× magnification. Top, Co-*C*; bottom, CoRu-*C*.

3.7. Reaction Rate

The rate of CO conversion on the pretreated catalyst samples is shown in Table 1. It can be seen that the rate of CO conversion during FTS decreased with the addition of water vapor during reduction. Since only Co metal has significant activity for FTS, these results are consistent with both the reducibility and H_2 chemisorption results. No significant change in product distribution was observed.

4. DISCUSSION

The BET surface areas of the catalysts in this study did not change significantly after the various pretreatments. It is clear that the various pretreatments in this study had little effect on surface area of the alumina support. Thus, changes in catalyst characteristics in this study were not caused by any change in total surface area of the catalysts.

In order to determine the bulk crystalline phases of the catalysts, XRD was performed. As seen in Fig. 1, the XRD peaks of the alumina support were present in all catalyst samples as broad peaks. The XRD patterns for Co and CoRu catalysts were identical for the same pretreatments, as shown in Fig. 1. Diffraction peaks of Co_3O_4 were observed for Co-*C* and CoRu-*C*. No XRD peaks of the Ru promoter were detected because Ru was present in such a small amount (0.5 wt%) and was well dispersed on the catalyst surface. After reduction and passivation, the diffraction peaks of Co_3O_4 were not apparent for Co-*RP*, Co-*RWP*, CoRu-*RP*, or CoRu-*RWP*. The diffraction peaks for CoO

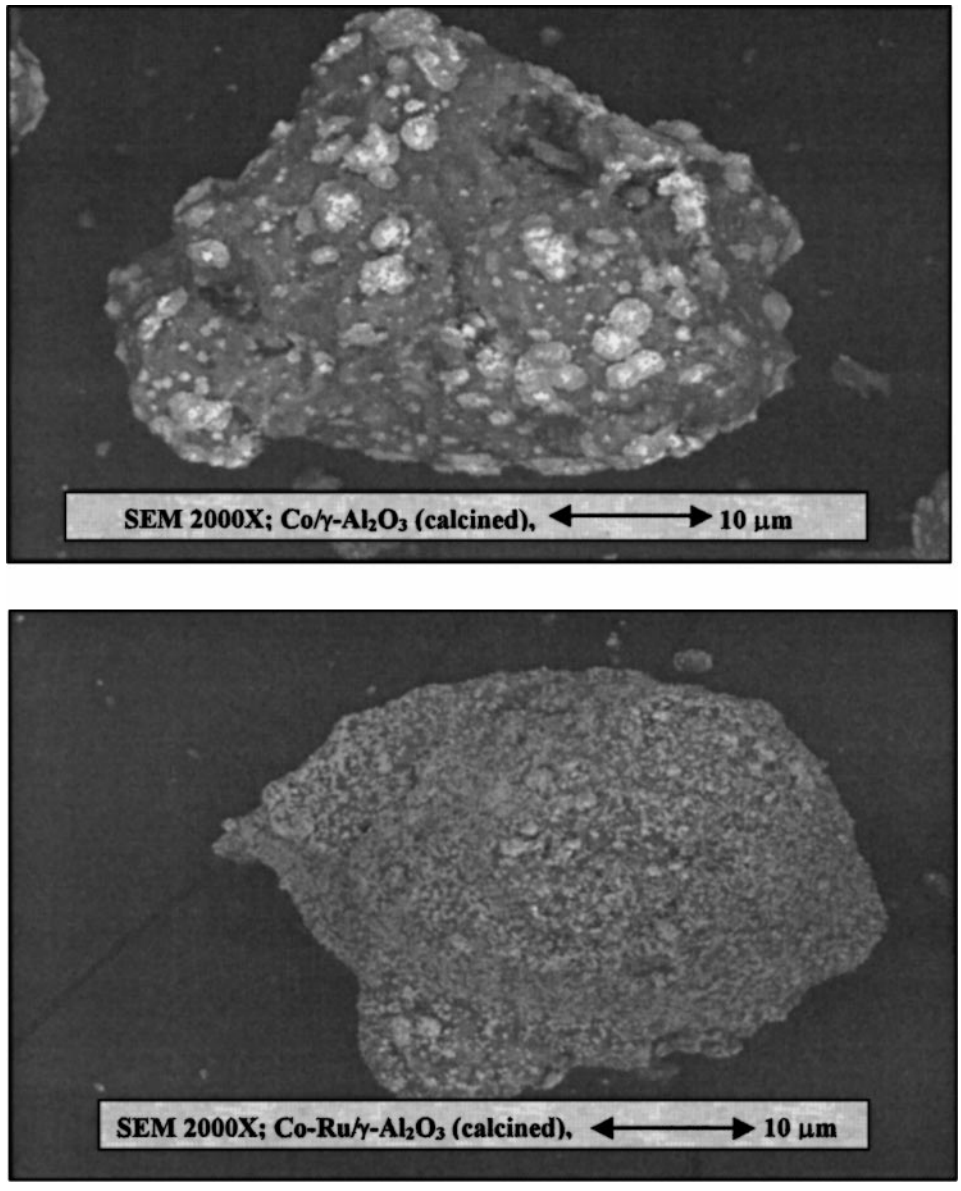

FIG. 4. SEM of the calcined Co/γ-Al_2O_3 and CoRu/γ-Al_2O_3 catalysts at 2000× magnification. Top, Co-*C*; bottom, CoRu-*C*.

were, however, present. This indicates that Co_3O_4 in the calcined samples was reduced to Co metal and CoO during standard reduction at 350°C. Any Co_3O_4 formed during passivation was present in only very thin surface layers and was consequently XRD invisible. Because both $CoAl_2O_4$ and Co_3O_4 have a spinel structure, the XRD patterns for both materials are almost identical, as shown in Fig. 1. No evidence for $CoAl_2O_4$ was detectable for either Co or CoRu after any of the reduction pretreatment conditions. The diffraction peaks of cobalt metal could not be seen due to overlap with those for γ-Al_2O_3. XRD patterns were identical for both Co and CoRu after the same pretreatments where additional water vapor was and was not introduced during reduction, as shown in Fig. 1.

Raman spectroscopy provided additional results with the Co species present. The strong Raman bands of Co_3O_4 in Co-*C* and CoRu-*C* can be observed in Fig. 2. They confirm the XRD results that Co_3O_4 was present in the calcined catalyst samples. After reduction, the strong Raman bands of Co_3O_4 totally disappeared. Broad Raman bands between 400 and 750 cm^{-1} were observed in all reduced and passivated samples (including both *RP* and *RWP* samples). However, these broad Raman bands were not identical to those of CoO, Co_3O_4 (spinel), or $CoAl_2O_4$ (spinel). Thus, the board Raman bands between 400 and 750 cm^{-1} cannot be attributed to either the support, Co_3O_4, CoO, Co metal, or $CoAl_2O_4$ (spinel). It is suggested that these broad Raman bands represent a surface Co compound species

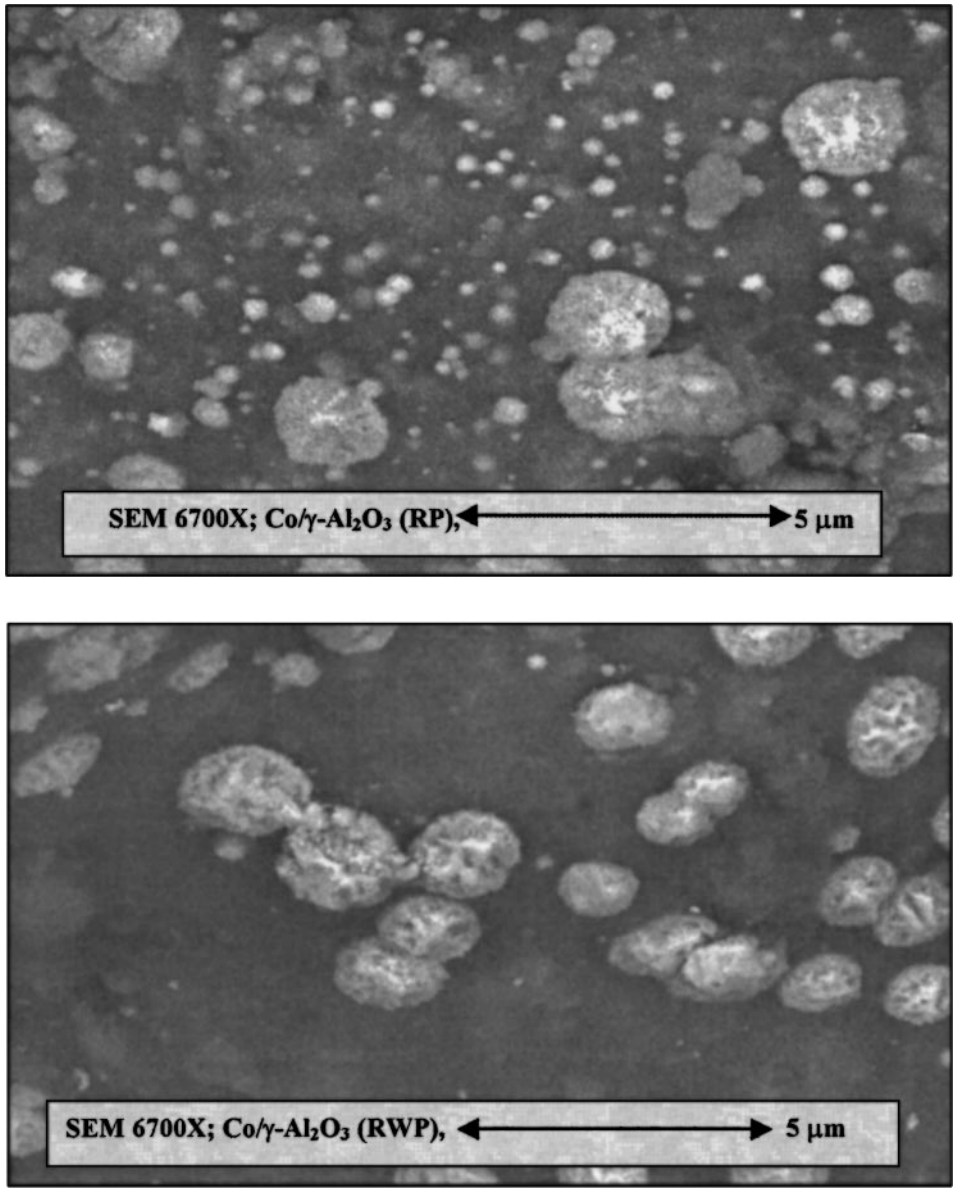

FIG. 5. SEM of the reduced and passivated Co/γ-Al_2O_3 catalyst at 6700× magnification. Top, Co-*RP*; bottom, Co-*RWP*.

related to Co strongly interacting with the alumina as a Co "aluminate." The identified Co aluminate is suggested to be different from $CoAl_2O_4$ (spinel) due to it being a nonstoichiometric surface Co aluminate compound. This highly dispersed Co aluminate ($Co–Al_XO_Y$) may be formed, possibly, by Co atom migration into the alumina matrix and is detectable using Raman spectroscopy but not XRD.

It is known that there are two steps for the reduction of bulk Co_3O_4 (13, 21–25). The first step is the reduction of Co_3O_4 to CoO and then that of CoO to Co metal. However, the two reduction steps may not always be observed as separate peaks in TPR (22–25), as seen in Fig. 7 for the reduction of bulk Co_3O_4. They can, however, be separated for bulk Co_3O_4 by adding water vapor during TPR (7). In addition, it has been found that often, due to interactions between Co_3O_4 and support materials such as silica or alumina, TPR of supported Co_3O_4 can also manifest a separation of the two reduction steps (18, 25).

TPR profiles of the catalyst samples are shown in Fig. 7. There were three reduction peaks located at ca. 200, 300, and between 400 and 750°C (max. at 600°C) for Co-*C*. It has been suggested that the reduction peak at ca. 200°C is due to the decomposition of residual Co nitrate to Co_3O_4 (8, 22, 23). However, XRD and Raman spectroscopic results (shown in Figs. 8 and 9) for dried $Co(NO_3)_2/\gamma$-Al_2O_3 prior to calcination (the precursor for Co-*C*) show no detectable amounts of $Co(NO_3)_2$ remaining and only the existence of Co_3O_4. Previous results from our lab have proved that this

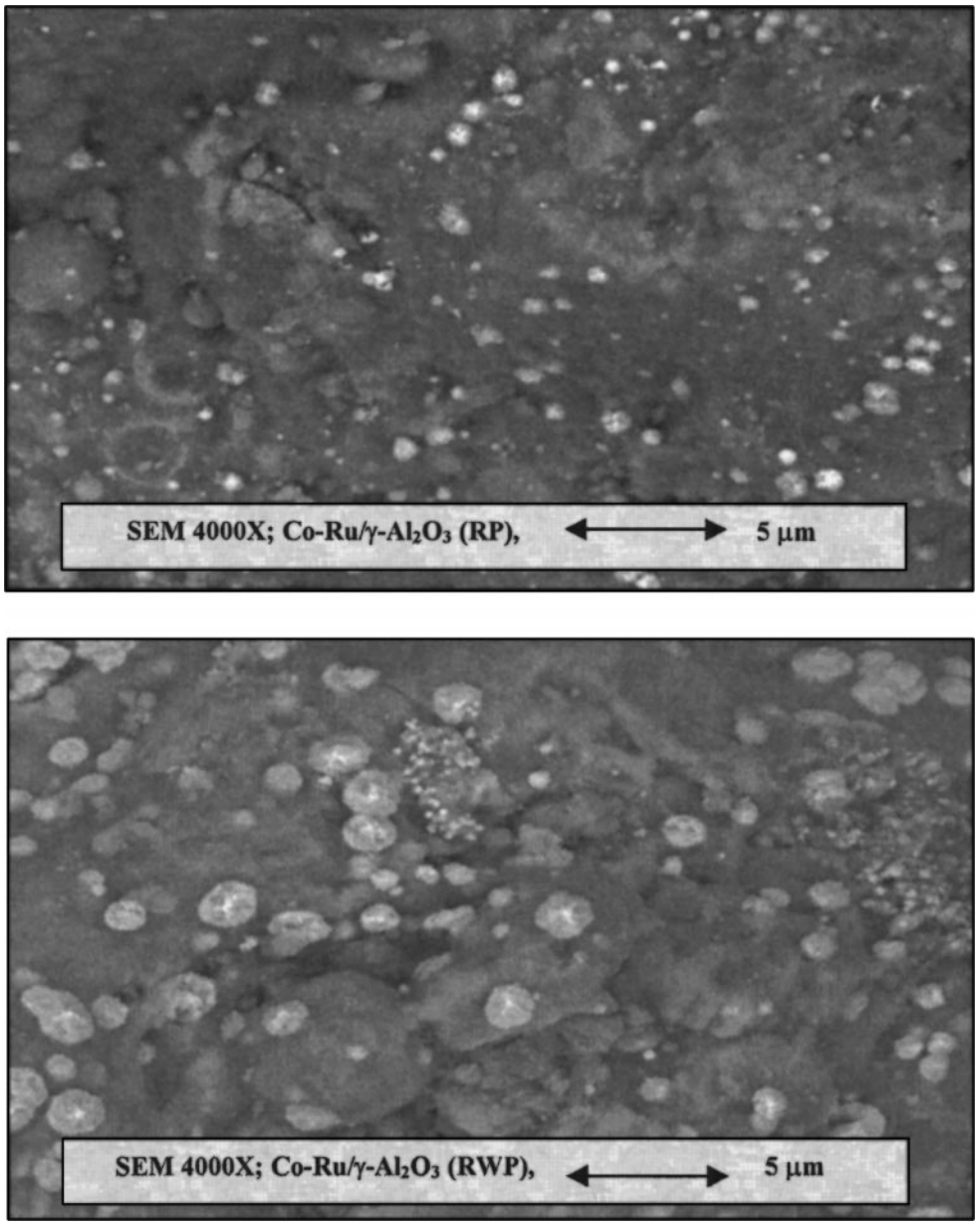

FIG. 6. SEM of the reduced and passivated CoRu/γ-Al_2O_3 catalyst at 4000× magnification. Top, CoRu-*RP*; bottom, CoRu-*RWP*.

peak for Co/γ-Al_2O_3 is due to decomposition of residual $Co(NO_3)_2$ (8).

TPR peak locations are affected by reduction kinetics. The kinetics of reduction can be affected by a wide range of variables, including particle size, support interaction, and reduction gas composition. The effects of particle size and support interaction can be superimposed on each other. Thus, while a decrease in metal oxide particle size can result in faster reduction due to a greater surface area/volume ratio, smaller particles may interact more with the support, slowing reduction.

It is suggested that the reduction of the unpromoted Co catalyst after various pretreatments can occur as shown in Fig. 10. For Co-*C*, the first reduction peak (at ca. 200°C) can be assigned to the decomposition of $Co(NO_3)_2$ (8, 22, 23), as has previously been shown for catalysts similar to this one (8). The second reduction peak (at ca. 300°C) is assigned to the reduction of Co_3O_4 to CoO and Co^0. The reduction peak at 400°–750°C (max. at 600°C) was clearly related to the reduction of Co strongly interacting with the support (Co_XO_Y–Al_2O_3) (23, 26–29), which can only be reduced at higher temperature.

The first low-temperature peak is not observed for a Co-*C* type catalyst if a longer calcination period of 14 h is used (8). Prolonged calcination or reduction and recalcination results in complete decomposition of any $Co(NO_3)_2$ present.

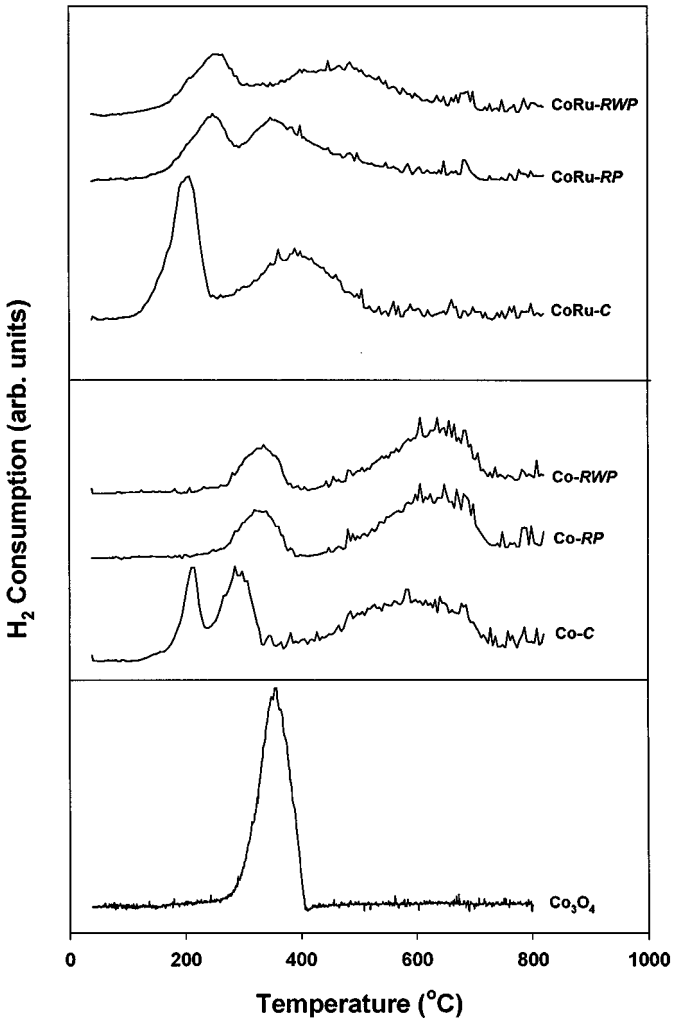

FIG. 7. TPR profiles of Co_3O_4, Co/γ-Al_2O_3, and CoRu/γ-Al_2O_3 catalysts.

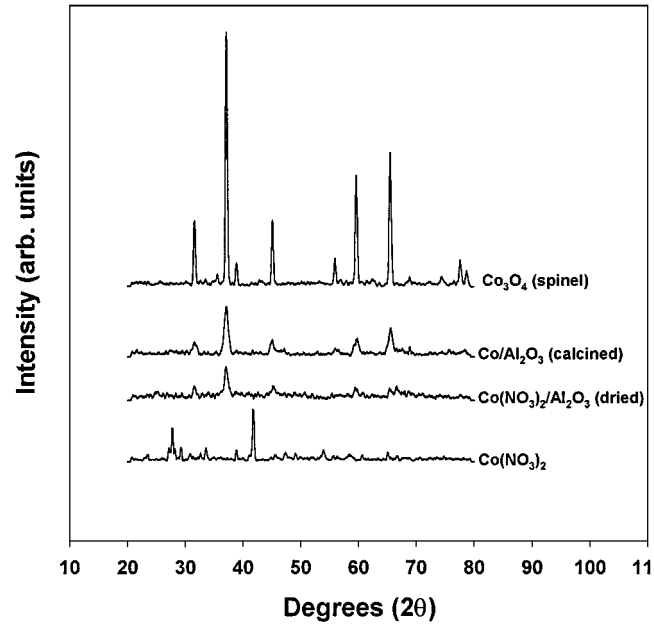

FIG. 8. XRD patterns of $Co(NO_3)_2$, Co_3O_4 (spinel), dried Co/γ-Al_2O_3, and calcined Co/γ-Al_2O_3.

As a result, the low-temperature (ca. 200°C) peak disappears after such treatments and only the second peak at ca. 350°C remains for Co-*RP* and Co-*RWP*. Reduction and recalcination probably causes sintering of Co_3O_4 and/or increased interaction with the support, resulting in a shift in the TPR peak to ca. 350°C for both Co-*RP* and Co-*RWP*. The reduction peak at ca. 600°C for Co-*RP* and Co-*RWP* was also about 20°C higher than that for Co-*C* due to stronger interaction between Co and the support induced by reduction and water effects on the Co_XO_Y–Al_2O_3 species.

TABLE 1

Reducibility, H_2 Chemisorption, and Reaction Rate during FTS for Co/γ-Al_2O_3 and for CoRu/γ-Al_2O_3 Catalysts after Various Pretreatments

Catalyst samples	Reducibility (%)[a] (30–900°C)	Total H_2 chemisorption[b] (μmol H_2/g cat.)	Overall dispersion (%)	Co^0 d_p[c] (nm)	Rate[d] (g CH_2/g cat./h) Initial	Rate[d] (g CH_2/g cat./h) SS
Co-*C*	83	—	—	—	0.149	0.112
Co-*RP*	58	484	5.7	15	0.130	0.072
Co-*RWP*	50	322	3.8	22	0.112	0.034
CoRu-*C*	98	—	—	—	—	—
CoRu-*RP*	86	662	7.8	11	—	—
CoRu-*RWP*	80	602	7.1	12	—	—

[a] The *RP* and *RWP* samples were recalcined at 300°C in air for 2 h before TPR measurement.

[b] Error = ±5% of measurement of H_2 chemisorption.

[c] Particle size is based on H_2 chemisorption and the amount of reduced cobalt [$d_p = 5/(S_{Co} \times \rho_{Co})$, where S_{Co} is the surface area of reduced Co/g of reduced Co].

[d] FTS was carried out at 220°C, 1 atm, and H_2/CO ratio = 2 (H_2/CO/Ar = 60/30/10 cc/min.).

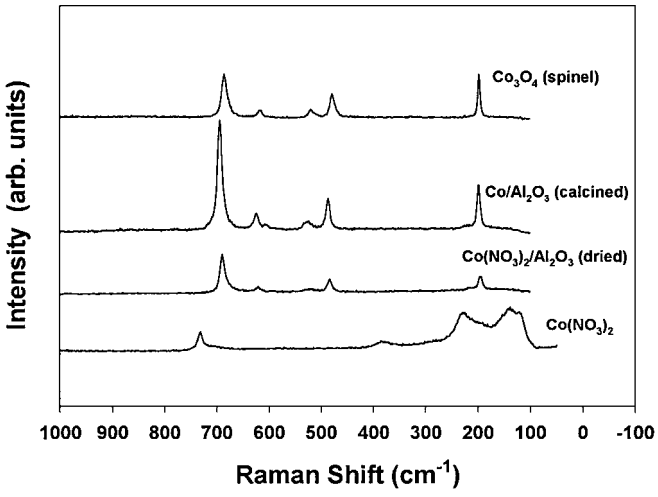

FIG. 9. Raman spectra of $Co(NO_3)_2$, Co_3O_4 (spinel), dried Co/γ-Al_2O_3, and calcined Co/γ-Al_2O_3.

It is suggested that the reduction in the Ru-promoted Co catalysts can occur as shown in Fig. 11. For CoRu-*C*, the two main reduction peaks were located at ca. 200°C and between 250° and 550°C (max. at 400°C). A lower temperature shoulder on the 200°C peak was observed due to the reduction of Ru_2O_3 to Ru^0 at ca. 160°C (30, 31). The reduction of Co_3O_4 to CoO and Co^0 then occurred around 200°C, along with some possible decomposition of residual Co nitrate. The higher temperature peak can be assigned to the reduction of Co strongly interacting with the support (Co_XO_Y–Al_2O_3) to Co^0.

For CoRu-*RP* and CoRu-*RWP*, two reduction peaks were also seen. However, the lower temperature peak was shifted about 60°C higher compared to that for CoRu-*C* probably due to sintering and/or increased interaction with the support caused by the reduction and recalcination prior to TPR measurement. It also had a low-temperature shoulder due to the initial reduction of Ru. The higher temperature peak located at ca. 380°C for CoRu-*RP* and at ca. 500°C for CoRu-*RWP* can again be assigned to the reduction of Co_XO_Y–Al_2O_3 to Co^0. This peak for CoRu-*RWP* at a higher temperature than that for CoRu-*RP* was undoubtedly caused by an increase in the interaction of Co with Al_2O_3 due to the presence a higher partial pressure of water vapor during reduction.

It can be observed that with Ru promotion, the reduction peaks of Co on alumina shifted to lower temperatures. This has been shown previously to be due to the Ru reducing at a lower temperature and then facilitating the reduction of Co (8–10).

The reducibilities during TPR from 30 to 900°C for the catalysts studied are shown in Table 1. The results indicate that the reducibility of samples increased with the addition of the Ru promoter and decreased with the introduction of additional water vapor during reduction. This indicates that a larger amount of the nonreducible Co aluminate (at temperatures $\leq$900°C) was formed during reduction in the presence of a "relatively" high partial pressure of water vapor (when 3% water vapor was added), leading to a lower reducibility. The addition of the Ru promoter resulted in an increase in reducibility of the catalyst. This might be explained in possibly one of two ways: (i) some of the Co strongly interacting with the alumina (Co_XO_Y–Al_2O_3) can be reduced at lower temperature when Ru is present and/or (ii) the Ru promotion can prevent the formation of the Co aluminate by minimizing the impact of water vapor on the formation of such compounds.

The results from H_2 chemisorption show that Ru promotion also results in an increase in the dispersion of the Co on the catalyst. This has been noted previously for noble metal promoted Co catalysts in general (2, 8–10, 13). The overall dispersion was found to decrease with the introduction of additional water vapor during reduction. This may be related to the loss of smaller Co patches/particles, as seen by SEM.

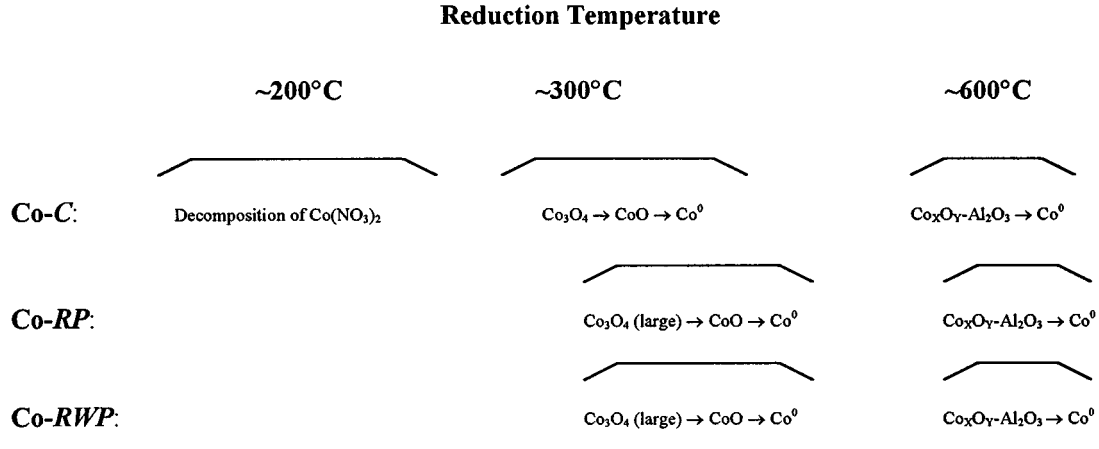

FIG. 10. Suggested reduction behavior of unpromoted Co catalysts after various pretreatments.

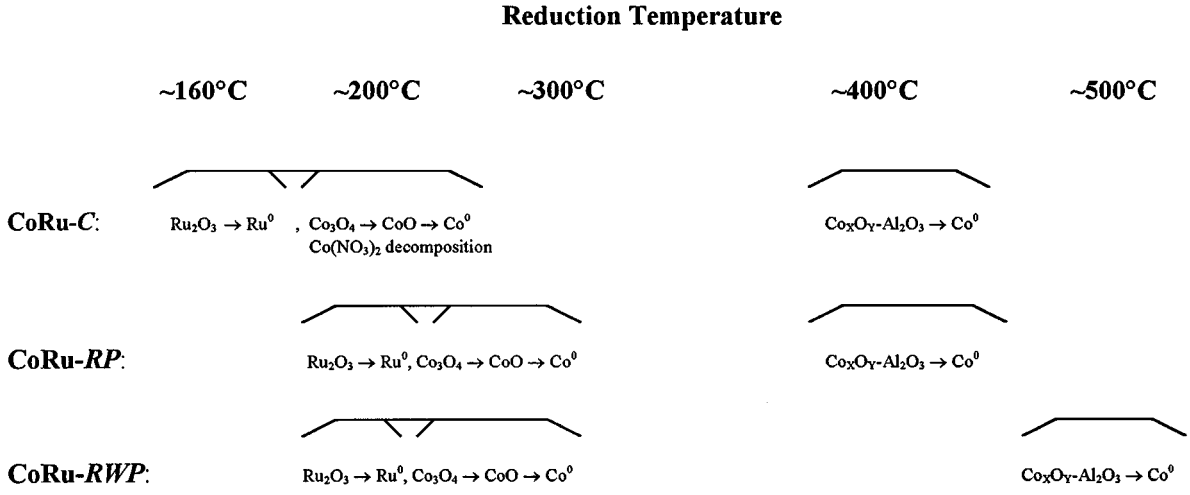

FIG. 11. Suggested reduction behavior of Ru-promoted Co catalysts after various pretreatments.

SEM and EDX gave information about the morphology and the elemental distribution of the alumina-supported cobalt catalysts after different pretreatments. It was confirmed that with the addition of Ru, Co is more dispersed on the catalyst surface. Comparing the particle size of Co obtained by SEM and H_2 chemisorption, it is obvious that the average particle size of Co^0 metal obtained from H_2 chemisorption (ca. 11–22 nm) is significantly smaller than the patches/particles seen by SEM (ca. 1–5 μm). In addition, SEM does not differentiate between Co metal, Co oxide, and Co aluminate. Thus, with SEM, only large dense patches of particles of Co metal and compounds can be detected. However, it must be noted that after reduction with and without added water vapor, significant differences were observed using SEM, as shown in Figs. 5 and 6. The disappearance of large numbers of smaller Co patches/particles can be seen after the introduction of additional water vapor during reduction. There are two possibilities: either water vapor can facilitate the migration of small Co particles, resulting in particle agglomeration (sintering), or it increases the diffusion of Co atoms from the smaller Co particles into the alumina. Considering the SEM, H_2 chemisorption, TPR, and Raman results, it would appear that both phenomena probably occur, with the latter being especially important and resulting in significant Co aluminate formation.

It was seen that the addition of water vapor during reduction also decreased the overall activity of the Co catalysts for FTS, which is related to the decrease in the reducibility and H_2 chemisorption of the catalysts. This is probably due to the fact that water vapor causes an increase in the amount of Co aluminate formation, resulting in a decrease in the amount of active Co metal available for the reaction.

5. CONCLUSIONS

Water vapor present during reduction has a major impact on alumina-supported Co catalysts, resulting in an increase in the amount of nonreducible Co aluminate (at temperatures $\leq$900°C) formed. This Co aluminate formation causes changes in the characteristics of Co catalysts, especially their reducibilities and overall activity during FTS. It is concluded that water vapor present during reduction possibly increases the amount of Co able to migrate into the alumina matrix, forming a highly dispersed Co aluminate and resulting in two broad Raman peaks between 400 and 750 cm^{-1}. This surface Co aluminate formed is different from $CoAl_2O_4$ (spinel).

The addition of Ru promoter to Co catalysts increases both the overall Co^0 dispersion and the reducibility. It is suggested that the Ru promoter not only facilitates the reduction of Co at lower temperatures, but also decreases the formation of Co strongly interacting with the alumina (Co_XO_Y–Al_2O_3) and nonreducible Co aluminate by minimizing the impact of water vapor on this formation. It is highly possible that this minimization is due to the effect of reduction at lower temperatures.

ACKNOWLEDGMENTS

The authors thank the Royal Thai government for financial support of Bunjerd Jongsomjit and Energy International, Inc., for providing the catalysts used in this study.

REFERENCES

1. Withers, Jr., H. P., Eliezer, K. F., and Mitchell, J. W., *Ind. Eng. Chem. Res.* **29**, 1807 (1990).
2. Iglesia, E., *Appl. Catal. A* **161**, 59 (1997).
3. Brady, R. C., and Pettit, R. J., *J. Am. Chem. Soc.* **103**, 1287 (1981).
4. Goodwin, Jr., J. G., *Prep. ACS Div. Pet. Chem.* **36**(1), 156 (1991).
5. Kogelbauer, A., Weber, J. C., and Goodwin, Jr., J. G., *Catal. Lett.* **34**, 259 (1995).
6. Schanke, D., Hilmen, A. M., Bergene, E., Kinnari, K., Rytter, E., Adnanes, E., and Holmen, A., *Catal. Lett.* **34**, 269 (1995).
7. Zhang, Y., Wei, D., Hammache, S., and Goodwin, Jr., J. G., *J. Catal.* **188**, 281 (1999).

8. Kogelbauer, A., Goodwin, Jr., J. G., and Oukaci, R., *J. Catal.* **160**, 125 (1996).
9. Belambe, A. R., Oukaci, R., and Goodwin, Jr., J. G., *J. Catal.* **166**, 8 (1997).
10. Iglesia, E., Soled, S. L., and Fiato, R. A., *J. Catal.* **137**, 212 (1992).
11. Blik, V. H. F. J., Köningsberger, D. C., and Prins, R., *J. Catal.* **97**, 210 (1986).
12. Martens, J. H. A., Blik, V. H. F. J., and Prins, R., *J. Catal.* **97**, 200 (1986).
13. Schanke, D., Vada, S., Blekkan, E. A., Hilmen, A., Hoff, A., and Holmen, A., *J. Catal.* **156**, 85 (1995).
14. Takeuchi, K., Matsuzaki, T., Arakawa, H., Hanaoka, T., and Sugi, Y., *Appl. Catal. A* **48**, 149 (1989).
15. Vada, S., Hoff, A., Adnanes, E., Schanke, D., and Holmen, A., *Top. Catal.* **2**, 155 (1995).
16. Iglesia, E., Soled, S. L., Fiato, R. A., and Via, G. H., *J. Catal.* **143**, 345 (1993).
17. Shipiro, E. S., Tkachenko, O. P., Belyatskii, V. N., Rudnyi, Y., Telegina, N. S., Panov, S. Y., Gryaznov, V. M., and Minachev, K. M., *Kinet. Catal.* **31**, 832 (1990).
18. Reuel, R. C., and Bartholomew, C. H., *J. Catal.* **85**, 63 (1984).
19. Ohtsuka, H., Tabata, T., Okada, O., Sabatino, L. M. F., and Bellussi, G., *Catal. Today* **42**, 45 (1998).
20. Li, J., and Coville, N. J., *Appl. Catal. A* **181**, 201 (1999).
21. Sexton, B. A., Hughes, A. E., and Turney, T. W., *J. Catal.* **97**, 390 (1986).
22. Arnoldy, P., and Moulijn, J. A., *J. Catal.* **93**, 38 (1985).
23. Hilmen, A. M., Schanke, D., and Holmen, A., *Catal. Lett.* **38**, 143 (1996).
24. Wang, W., and Chen, Y., *Appl. Catal. A* **77**, 223 (1991).
25. Lapidus, A., Krylova, A., Kazanskii, V., Borovknov, Z., Ratnousky, J., Zukal, A., and Jan, M. C., *Appl. Catal. A* **73**, 65 (1991).
26. Delmon, B., and Roman, A., *J. Catal.* **30**, 333 (1973).
27. Houall, M., Delannay, F., Matsuura, I., and Delmon, B., *J. Chem. Soc., Faraday Trans.* **176**, 2128 (1980).
28. Mile, B., Stirling, D., Zammitt, M., Lovell, A., and Webb, M., *J. Catal.* **144**, 217 (1988).
29. van'T Blik, H. F. J., and Prins, R., *J. Catal.* **97**, 188 (1986).
30. Hurst, N. W., Gentry, S. J., Jones, A., and McNicol, B. D., *Catal. Rev. Sci. Eng.* **24**(2), 233 (1982).
31. Betancourt, P., Rives, A., Hubaut, R., Scott, C. E., and Goldwasser, J., *Appl. Catal. A* **170**, 307 (1998).